Pergamon

Journal of Structural Geology, Vol. 16, No. 12, pp. 1691 to 1709, 1994
Elsevier Science Ltd
Printed in Great Britain
0191-8141/94 $7.00 + 0.00

0191-8141(94)E0011-M

Application of an automatic method for determining normal fault geometries

H. G. KERR and N. WHITE

Bullard Laboratories, University of Cambridge, Madingley Road, Cambridge CB3 0EZ, U.K.

(*Received* 4 *May* 1993; *accepted in revised form* 20 *January* 1994)

Abstract—An automatic method is used to determine the geometries of normal faults on depth-converted seismic reflection profiles from the Gulf of Mexico and from the North Sea. The general method has previously been tested on synthetic and sand-box data and assumes that the hanging wall deforms within the plane of section by a combination of arbitrarily inclined, bulk simple-shear and differential compaction. The range of possible solutions is systematically investigated using inverse modelling. We assume that the fault surface does not significantly change shape during deformation. However, inversion of flexural forward models shows that when the fault surface does change shape, the misfit function at an automatically determined solution is unacceptably large and featureless. Consequently, spurious solutions, obtained when the principal assumptions break down, can be identified. The approximations used in modelling the effects of differential compaction are justified by a range of appropriate synthetic models. We reiterate that the inversion procedure is dependent upon careful identification of: (a) two or more deformed horizons within the hanging wall; and (b) the regional levels of deformed horizons before deformation. The numerical stability of the scheme is demonstrated by inverting synthetic data to which random and systematic noise have been added. The solutions we have obtained are good and indicate that the method works regardless of the scale and shape of the faults. Throughout, we emphasize the importance of combining inverse theory with a simple kinematic model in order to investigate the solution space and the resolution of the model parameters obtained.

INTRODUCTION

THE arbitrarily inclined shear model proposed by White *et al.* (1986) and now generally accepted (see e.g. Roberts *et al.* 1990), uses geometry of deformed hanging wall horizons to determine the geometry of fault surfaces at depth. This approach is appropriate since seismic reflection profiling can accurately image hanging and footwall beds but is often poor at directly imaging fault surfaces at depth. Using the well-known techniques of inverse theory, Kerr & White (1992) tested this model on a large number of two-dimensional laboratory-modelled faults, showing that the main fault surface could always be determined automatically. This paper is concerned with applying the inverse model to listric and 'domino-style' normal faults imaged on seismic reflection profiles. Previously, it was argued that section-balancing schemes, similar to this one, are only applicable to surficial normal faults within the sediment fill of a basin (Roberts *et al.* 1990). Here we demonstrate that, if allowance is made for rotations about the horizontal axis, the model is also applicable to major domino-style normal faults whose hanging walls may also be deforming internally.

A full description of the model is given in White (1992) and Kerr & White (1992). The main assumptions are that: (a) the hanging wall deforms within the plane of the two-dimensional section by a combination of arbitrarily inclined, bulk simple shear and differential compaction; (b) the fault stays the same shape as deformation proceeds; (c) the unfaulted geometry of two or more horizons are known; and (d) the fault portion between terminations of hanging wall and footwall horizons is known. Deformation is described by three parameters: α, the inclination of shear planes, measured with respect to the vertical (positive when antithetic to main fault); ϕ_o the porosity of sediments at the regional level of the uppermost horizon; and λ, the porosity decay length. These three parameters and the main fault surface are unknown, although bounds may sometimes be placed on their values. The correct fault shape and values for the deformation parameters are obtained by searching the solution space until the misfit between the faults predicted from each of the hanging wall horizons is minimized.

In general, extension is not necessarily parallel to the plane of the section and so the assumption of plane strain may be incorrect. Kerr *et al.* (1993) have thus generalized the two-dimensional model and developed a three-dimensional procedure which can invert for the direction of extension within the horizontal plane as well as the three-dimensional fault geometry. This model has been successfully tested on synthetic data, on a series of three-dimensional sand-box experiments, and on three-dimensional seismic reflection data (Kerr *et al.* in preparation). In instances where there has been oblique extension but where the fault surface does not change geometry dramatically along strike, the two-dimensional method used in this paper is able to determine the correct fault surface (Kerr *et al.* 1993).

Sand-box analogues of normal faulting provide a good initial test for section-balancing models. However, in applying the inversion scheme to geological faults, several complicating factors not present in sand-box models may lead to ambiguous results. Knowledge of circumstances when the inversion scheme is likely to fail is of

great importance since it means that spurious solutions can be identified. Consequently, before the method is applied to seismic reflection data, a number of general complications must be considered.

COMPLICATIONS

Fault surface changing shape during deformation

Listric faults on seismic reflections commonly show a deformed hanging wall and a relatively undeformed footwall. This observation gave rise to the assumption that the footwall remains rigid (i.e. the fault itself does not change shape) as extension proceeds (Wernicke & Burchfiel 1982, Bally 1983).

Seismological studies of aftershocks of large-magnitude basement-extending normal faults demonstrates that some footwall deformation does occur and consequently the fault surface does change shape during deformation (Soufleris *et al.* 1982, King *et al.* 1985, Lyon-Caen & Molnar 1986, Richins *et al.* 1987). However, footwall deformation may not be very significant as the majority of aftershocks occur in the hanging wall rather than in the footwall and in any case the cumulative seismic moment of all aftershocks is very small compared to that of the main shock (King *et al.* 1985).

Geodetic measurements following the 1983 Borah Peak earthquake (Stein & Barrientos 1985) indicate that co-seismic deformation is accommodated by footwall uplift as well as hanging wall subsidence. It was also observed that uplift and subsidence decrease exponentially away from the fault. Similar observations, although less complete, have been made following other normal fault earthquakes. For example, geodetic profiles for the 1928 Bulgaria earthquake (Jankhof 1945, Richter 1958), for the 1954 Fairview Peak earthquake (Whitten 1957), and for the 1959 Hegben Lake earthquake (Myers & Hamilton 1964) all show a pattern of uplift and subsidence similar to the Borah Peak earthquake. It is believed that a similar deformation field is produced by seismic slip on small faults. From these observations, Gibson *et al.* (1989) proposed a set of empirical relationships which could be used to model hanging wall subsidence and footwall uplift adjacent to a planar normal fault. However, this model is only applicable to faults in which co-seismic deformation has been the dominant deformation process since inter-seismic, and more importantly pre-seismic, phases of deformation are ignored.

We have used a simplified version of the flexural cantilever model (Kusznir *et al.* 1991) in synthetic forward modelling to investigate how a fault surface which changes shape during extension will effect solutions obtained by inverse modelling. For our purposes, the significance of flexure is that it allows the fault surface to change shape during deformation. Reservations about general relevance of flexural models for matching the topography generated during the syn-rift phase of extension are considered below. The flexural response is controlled primarily by the flexural rigidity of the plate, which is usually described as an effective elastic thickness, τ_e. The smaller the value of τ_e, the more the fault surface changes shape during deformation.

In Fig. 1, an initial planar fault and three horizontal beds are deformed by successive increments of 15 m of extension until 1.5 km of extension are achieved. In each increment, hanging wall deformation is modelled by a combination of inclined simple shear and differential compaction with $\alpha = 30°$, $\phi_0 = 45\%$ and $\lambda = 2$ km. The flexural response is calculated after each increment of displacement for a range of values of τ_e (Figs. 1b–d). The inverse model of Kerr & White (1992) is then applied to the final bed geometries, using Powell's method (Press *et al.* 1986) to locate the minimum misfit. In Fig. 2, the forward flexural model is applied to an initially listric fault with the deformation parameters set to the same values as before.

It is clear that when the fault surface changes shape significantly during deformation, the predicted faults are not coincident and the misfit function is uniformly large. This failure highlights a very significant feature of the inversion scheme: if no adequate solution can be found (i.e. if the misfit function is uniformly large and featureless), then inferences may be drawn concerning the underlying assumptions stated above. In this case, the fault surface has obviously changed shape significantly during deformation. Conversely, models which use the geometry of one or more horizons to forward model the solution without examining the shape of the misfit function may yield misleading results. Note that at higher values of τ_e, the fault surface still changes shape but now inversion produces adequate solutions.

Differential compaction

Normal faults typically occur within sediments where compaction is likely to be significant. As extension proceeds and more sediment is deposited, water is expelled and the resultant compaction can account for up to 30% of the total strain (Ramsay 1967). It has been suggested (e.g. Sclater & Christie 1980, Wood 1981) that compaction can be modelled empirically as a uniaxial process with a vertical axis of shortening. However, removing the effects of vertical compaction requires *a priori* knowledge of the fault geometry. Therefore the inverse model, in which the fault geometry is generally unknown, cannot be solved (Waltham 1990). The simplest approximation is to constrain the axis of shortening parallel to the direction of shear (White *et al.* 1986).

It is important to determine how accurate this approximation is likely to be. To do so, we have produced a forward model where compaction is modelled correctly (i.e. vertically; Fig. 3). Before deformation, the porosity, $\phi(y)$, is calculated at regular intervals within the hanging wall using the following empirical relationship (e.g. Sclater & Christie 1980):

$$\phi(y) = \phi_0 \exp(-y/\lambda), \quad (1)$$

where y is the depth of a point below the regional level of

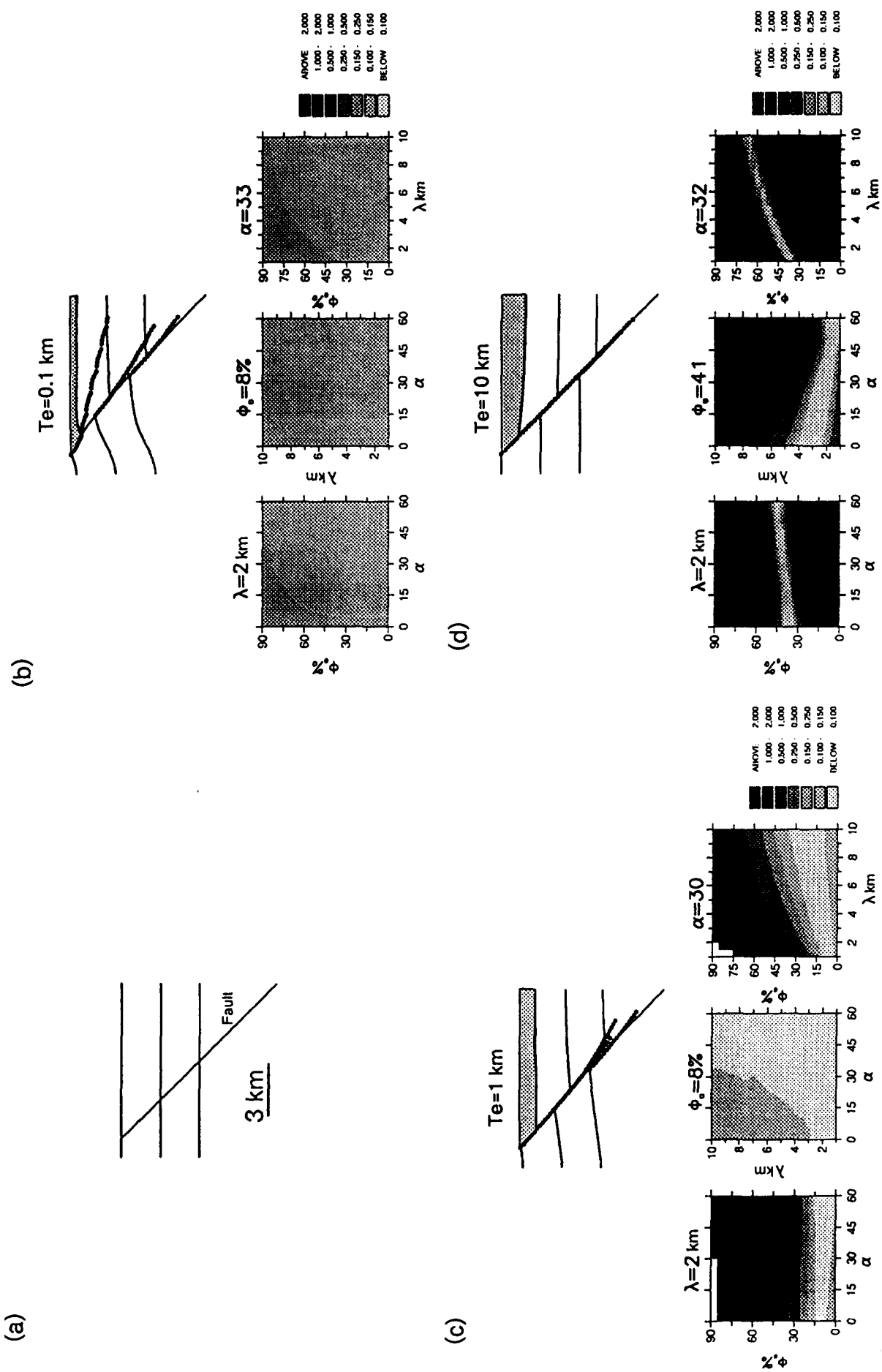

Fig. 1. Forward model adapted to include flexural response due to loading/unloading of footwall. (a) Initial fault and bed geometry with scale bar. (b)–(d) Solid lines indicate bed geometries generated by forward flexural model with $\alpha = 30°$, $\phi_0 = 45\%$, $\lambda = 2$ km. τ_e set to different values as indicated. Shading above first bed indicates flexurally compensated sediment load. In each case dotted lines are locations of fault surfaces calculated at the solution. Contour plots of misfit function at location of solution are shown (see Kerr & White 1992 for further details).

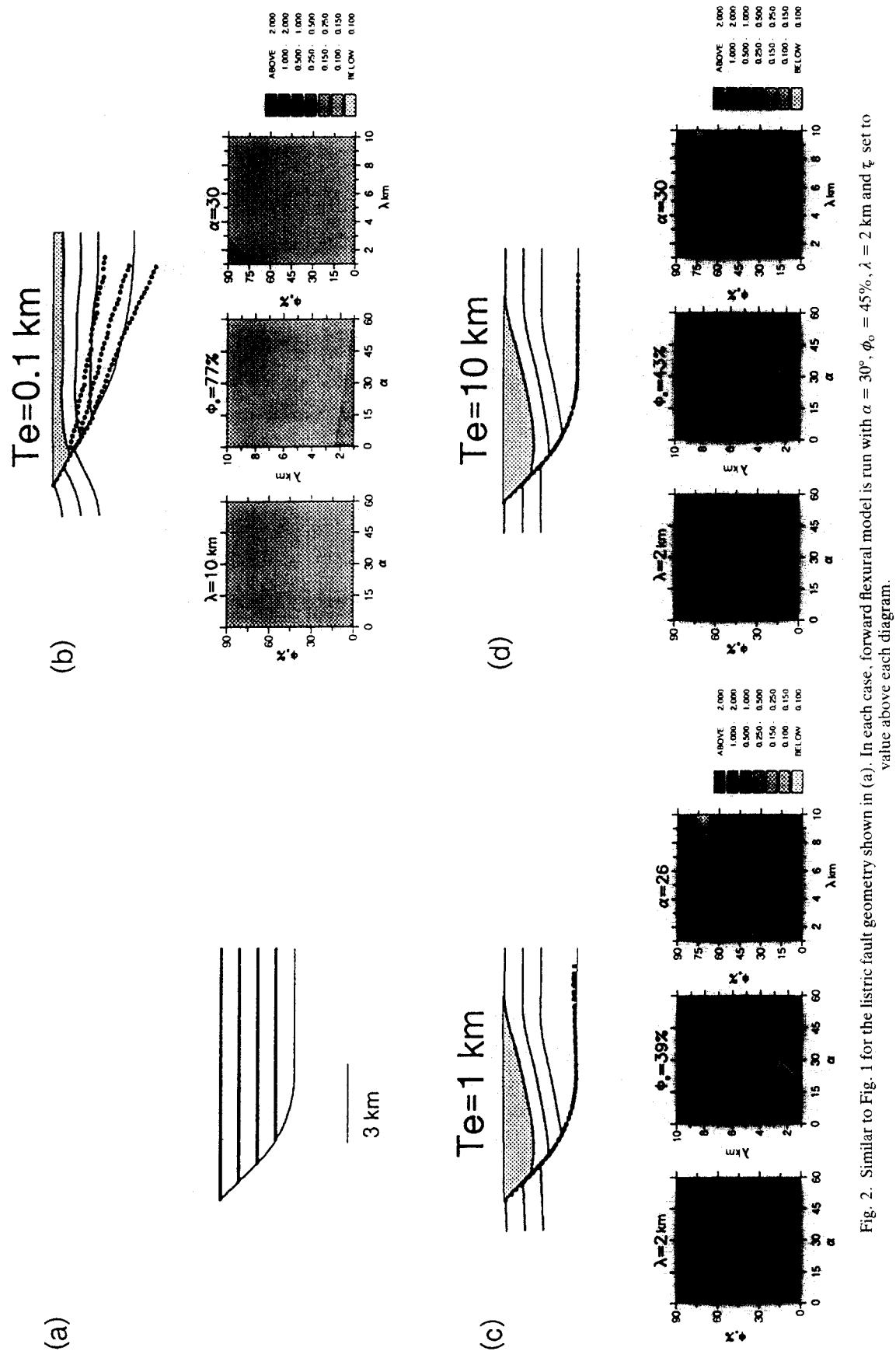

Fig. 2. Similar to Fig. 1 for the listric fault geometry shown in (a). In each case, forward flexural model is run with $\alpha = 30°$, $\phi_o = 45\%$, $\lambda = 2$ km and τ_e set to value above each diagram.

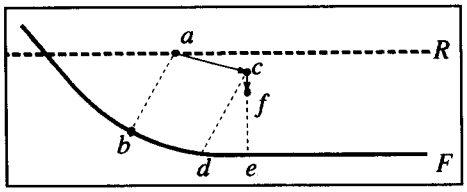

Fig. 3. Geometrical relationship for inclined simple shear and differential compaction with axis of shortening vertical. Solid line is fault surface. Dashed line is regional level, R, of horizontal bed which is deformed by simple shear such that a is translated to c. Lengths $|ab|$ and $|cd|$ are equal. Hanging wall then compacted vertically. Length $|ce|$ shortens to $|fe|$. f is position of deformed bed. See text for further details.

the uppermost horizon, λ is the porosity decay length, and ϕ_0 is the porosity at the regional level of the uppermost horizon. The hanging wall is then extended by a small increment of the total extension and deformed by simple shear such that a point a initially at the regional level, R, is translated to c. The porosity of the material at c and the material vertically below it (i.e. between c and e) is smaller than that before the deformation occurred. The decrease in porosity with burial will result in length $|ce|$ shortening to $|fe|$. The amount of solid material between c and e is equivalent to the amount of solid material between f and e. Thus

$$(e - c)(1 - \phi_1) = (e - f)(1 - \phi_2), \qquad (2)$$

where ϕ_1 is the average porosity between c and e, and ϕ_2 is the average porosity between f and e including the decrease in porosity due to burial by movement on the fault. Hence equation (2) may be used to calculate f, the compacted position of the bed. The compacted bed is then deformed by further increments of the total extension in the same way. This form of the forward model cannot be used to pose the inverse since the position of e is unknown (i.e. we cannot assume *a priori* information concerning fault geometry).

Three examples of vertical compaction forward models, each of which will subsequently be inverted, are shown in Fig. 4. Four initially horizontal beds (Fig. 4a) are deformed by successive increments of 30 m of extension until an extension of 1.5 km is achieved. The value of α is increased by 15°, in each forward model, from $\alpha = 15°$ in Fig. 4(b) to $\alpha = 45°$ in Fig. 4(d). $\phi_0 = 45\%$ and $\lambda = 2$ km in all the forward models. When the inverse procedure is applied, the solutions are excellent: in each case there is a close fit between the predicted faults and the actual fault surface. Hence, although the axis of shortening is vertical in the forward model, the inverse model is able to adequately represent deformation by modelling the axis of shortening parallel to the direction of shear. We see no need to model compaction in a more complex fashion at this stage. In future, regional estimates of ϕ_0 and λ could be used to provide useful bounds for these parameters.

An alternative method of forward modelling hanging wall deformation was proposed by Waltham (1990) in which the axis of shortening is constrained to be parallel to the main fault surface. The conservation of mass provides the main constraint which, for a flowing medium, requires that the equation of continuity (Birkhoff 1955) is satisfied:

$$\nabla \cdot (\rho \mathbf{v}) + \frac{\partial \rho}{\partial t} = 0. \qquad (3)$$

ρ is the density, $\mathbf{v}$ is vector velocity, and t is time. Given the directions of movement at specified grid points, equation (3) may be solved for the magnitude of the velocity using a finite-difference scheme. Once displacement rates and directions have been found, deformation is calculated by summing displacements over appropriate increments of time. This scheme is the most general model for calculating hanging wall deformation. However a consequence of such generality is that the inverse model, which predicts fault geometry from hanging wall deformation, cannot be easily formulated. Also it seems unlikely that modelling compaction parallel to the fault surface is realistic since compaction must then cause a significant proportion of the displacement along the fault.

Waltham's (1990) finite-difference scheme is used in Fig. 5 to generate three different hanging wall geometries. The initial bed and fault shapes in Fig. 5(a) are used and 1.5 km of extension is added with $\phi_0 = 45\%$ and $\lambda = 2$ km. As before, the value of α is increased by 15° in each forward model from $\alpha = 15°$ in Fig. 5(b) to $\alpha = 45°$ in Fig. 5(d). When these models are inverted, the deformation parameters located by Powell's method differ from the input values. However the predicted fault surfaces all coincide with the true fault surface. Therefore although a different mechanism of deformation was used in the forward model, once again the inverse model is able to adequately represent the deformation.

Finally, we come to the problem of post-rift burial. This process must be considered since it affects most of seismic reflection examples used in this paper and in the literature. When burial occurs, both hanging and footwall strata undergo further compaction changing both the regional level of each horizon, the shape of the beds, and the shape of the fault. Rather than altering the observed geometries by backstripping each section, we prefer to investigate directly the consequences of such burial using simple synthetic models where the same model is buried under an increasing mass of sediment (Fig. 6). Burial must cause a decrease in bed thickness and the geometry of the fault itself is also modified. However, burial is generally large and uniform (2–4 km with wavelengths of 10–100 km) and so the regional level of each bed suffers very little change in dip. Hence the four solutions calculated by inversion hardly differ. We have carried out similar tests on a wide range of fault and bed geometries and in all cases the results indicate that we are justified in ignoring the affects of post-rift burial.

Resolution of deformed hanging wall horizons

Accurate interpretation of stratigraphy on seismic reflection profiles is not always straightforward. Hori-

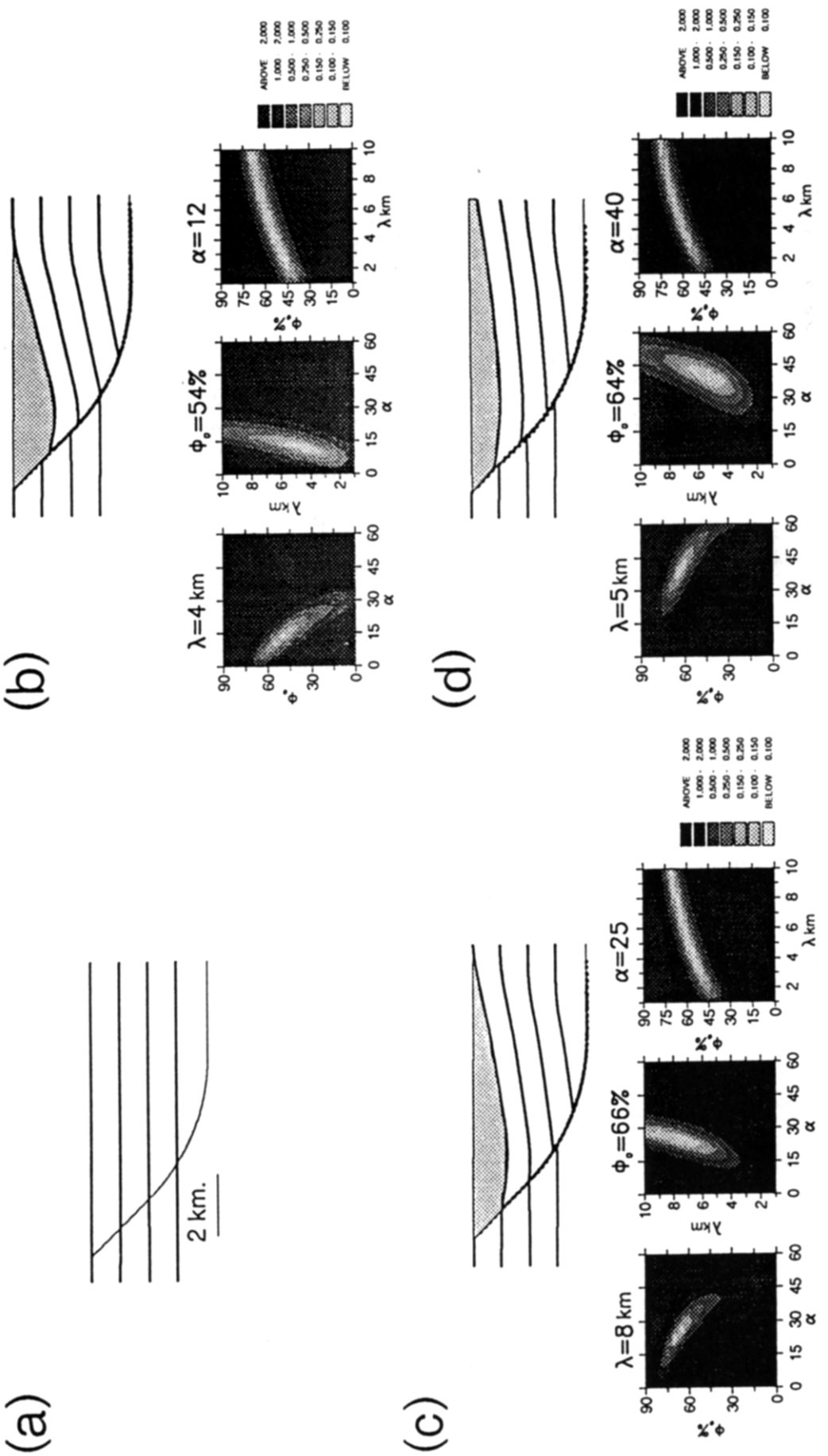

Fig. 4. Deformation of four horizontal beds in (a) is forward modelled by a combination of inclined simple shear and vertical differential compaction with $\phi_o = 45\%$ and $\lambda = 2$ km, in each case, and α increased by 15°, in each forward model, from $\alpha = 15°$ in (b) to $\alpha = 45°$ in (d). Calculated fault surfaces at the solution are indicated by dotted lines. Shading above first bed indicates sediment infill. Contoured slices through misfit function shown for each case.

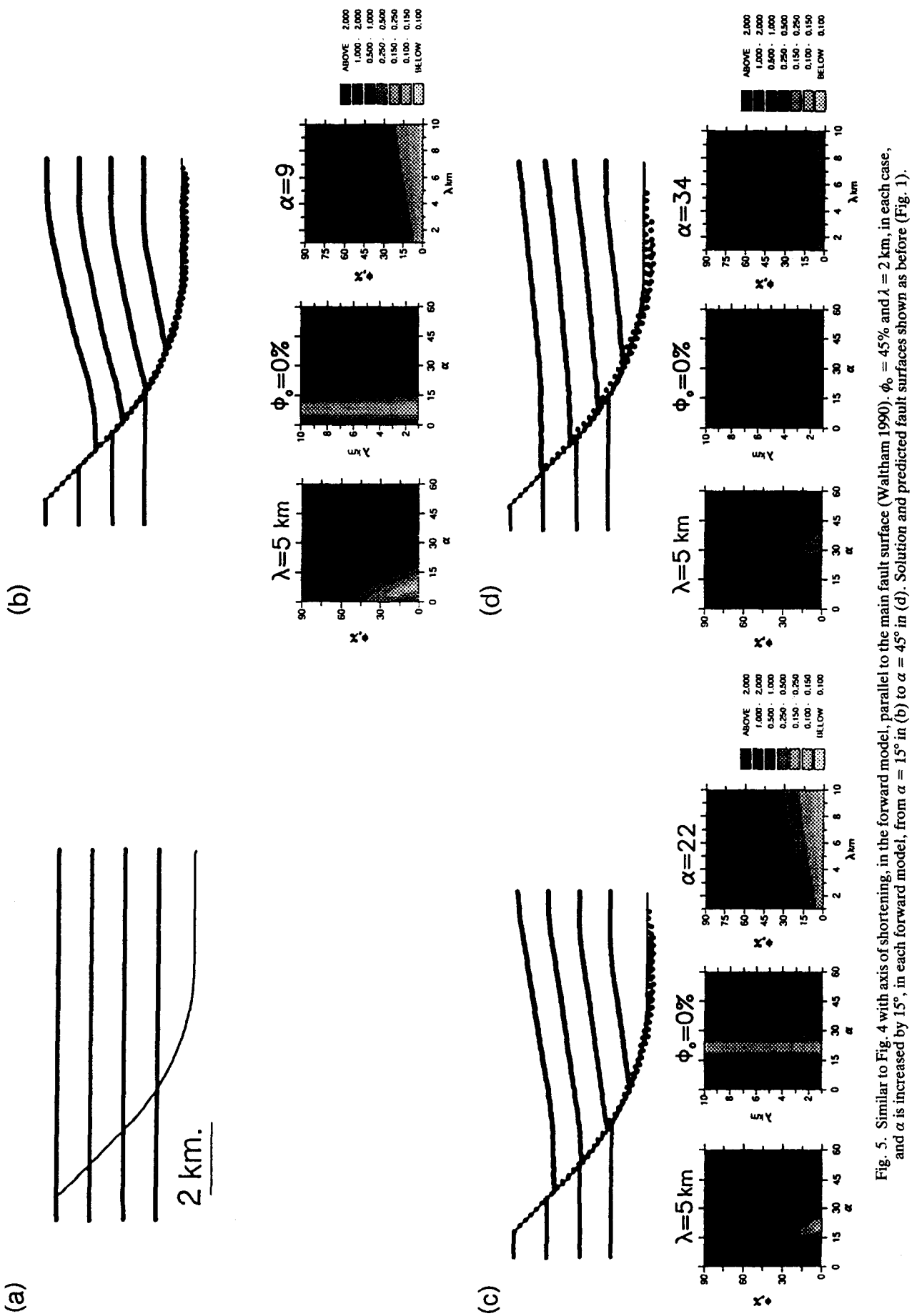

Fig. 5. Similar to Fig. 4 with axis of shortening, in the forward model, parallel to the main fault surface (Waltham 1990). $\phi_0 = 45\%$ and $\lambda = 2$ km, in each case, and α is increased by 15°, in each forward model, from $\alpha = 15°$ in (b) to $\alpha = 45°$ in (d). *Solution and predicted fault surfaces shown as before* (Fig. 1).

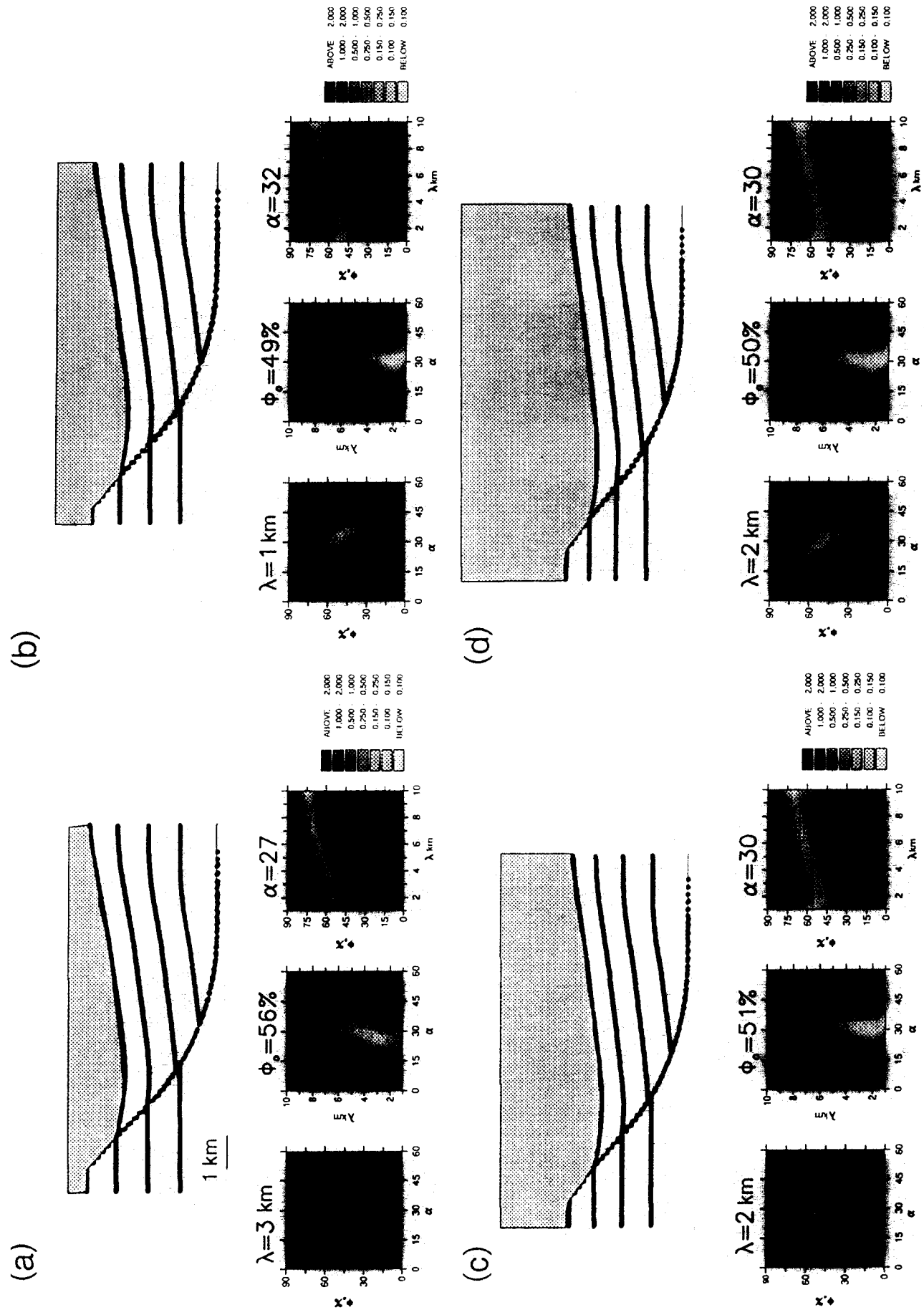

Fig. 6. Investigation of effects of post-rift burial. Forward model was run with $\alpha = 30°$, $\phi_0 = 45\%$, and $\lambda = 2$ km. Axis of shortening for compaction is vertical. After extension, further burial indicated by shading. See Fig. 4 for further details.

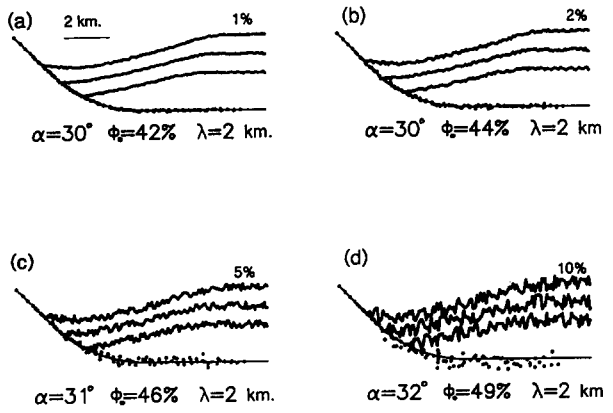

Fig. 7. Random noise added to synthetic data generated with $\alpha = 30°$, $\phi_0 = 45\%$, $\lambda = 2$ km. (a)–(d) Maximum amount of noise (indicated above figures) is a percentage of vertical distance between top and bottom of fault (range). Solutions and predicted fault surfaces shown as before (see Fig. 1).

zons are often disrupted by minor faults making correlation difficult. Here the effect that such interpretational error has on the inversion model is investigated in two ways. First, random noise is added to the deformed hanging wall horizons. Secondly, regional levels of deformed hanging wall horizons are systematically displaced.

(a) *Random noise.* The inversion scheme requires that deformed hanging wall horizons are accurately interpreted and digitized. We can examine the effects that random noise has by adding it to synthetic models which are then inverted. In Fig. 7, synthetic data was generated by the forward model with $\alpha = 30°$, $\phi_0 = 45\%$ and $\lambda = 2$ km. The maximum amount of noise is determined as a percentage of the range of the data (i.e. the vertical distance between the top and bottom of the fault). In the examples shown, a 1% error is equivalent to misplacing the horizon by 32 m. The solutions clearly show that the inversion procedure is stable to random noise.

The possible range of parameter values obtained in the presence of random noise can be investigated by adding different random noise to the synthetic data 200 times in order to generate 200 different hanging wall geometries. The maximum amount of noise added is 2% of the range (the same as Fig. 7b). Inverted solutions are plotted in parameter space and confidence limits assigned to parameter values extracted by inversion. This 'Boot-strap method' (Press *et al.* 1986) yields Monte Carlo estimates of the likely error for a given parameter set. A confidence region or interval summarizes the probability distribution of errors in parameter estimation and is just that region of space that contains some percentage of the total probability distribution (Press *et al.* 1986). In our case, the 99% confidence region for each pair of parameters is small indicating that our inversion scheme is well-posed in the sense of Parker (1977) (Fig. 8). For planar faults, we find, as anticipated, that the constraint upon α is poor (see also Kerr & White 1992). More formally, the directions and lengths of the principle axes of the circumscribed ellipses correspond to the eigenvectors and the reciprocals of the eigenvalues of the Hessian matrix in the vicinity of the identified solution.

(b) *Systematic noise.* We assume that the regional levels of each deformed hanging wall horizons can be correctly identified from the intersection of footwall horizons with the fault. In practice, the correlation of horizons from the hanging wall to the footwall can be difficult and it is important to know how sensitive the model is to systematic variation in regional level. Once again, synthetic modelling is used to investigate the effect that fixing incorrect regional levels has on the inversion scheme (Fig. 9). First, the forward model is run with $\alpha = 30°$, $\phi_0 = 45\%$ and $\lambda = 2$ km. Regional levels of all beds are then shifted systematically, as a percentage of the range, from their correct position. As before, a 1% error is equivalent to misplacing the regional level by 32 m. Figure 9 demonstrates that to predict the correct fault trajectory the regional levels of the hanging wall horizons must be carefully identified. Significant error in regional level causes the predicted fault surface to dip incorrectly at depth. The difference between the predicted and true fault surface is greater when regional levels are fixed too deep. If, however, regional levels are fixed below their actual locations the predicted faults intersect the hanging wall strata. Such solutions are physically unrealistic and indicate that the correlation of horizons between the hanging wall and footwall is incorrect.

If correlation from hanging wall to footwall is very poor and if the geometry of the fault is already known, then it is possible to turn the inverse problem around in order to determine stratal correlation as opposed to fault geometry.

Rotating fault blocks and the flexure problem

Normal faulting combined with a rigid-body rotation (known as 'domino-style' faulting) has been recognized in many regions of extensional tectonics (Ransome *et al.* 1910, Proffett 1977, Le Pichon & Sibuet 1981). Usually, domino-style faults are assumed to be approximately planar (Le Pichon & Sibuet 1981, McKenzie & Jackson 1983). Roberts *et al.* (1990) argue that since the footwall as well as the hanging wall has deformed the application of geometric section-balancing techniques to this style of faulting will result in incorrect fault geometries being predicted.

Roberts & Yielding (1991) concede that a domino-type fault model, where all fault blocks rotate about a horizontal axis, may be appropriate for extensional sedimentary basins such as the North Sea. However, they point out that the domino model yields unsatisfactory solutions for deformation at basin margins since a marginal fault is the last fault in an array and so its footwall cannot remain static during deformation. Instead of a domino-type model, Roberts & Yielding (1991) propose that the flexural-cantilever model (Kusznir *et al.* 1991) be used since it allows a unified treatment of both basinal and marginal faults. In contrast, we

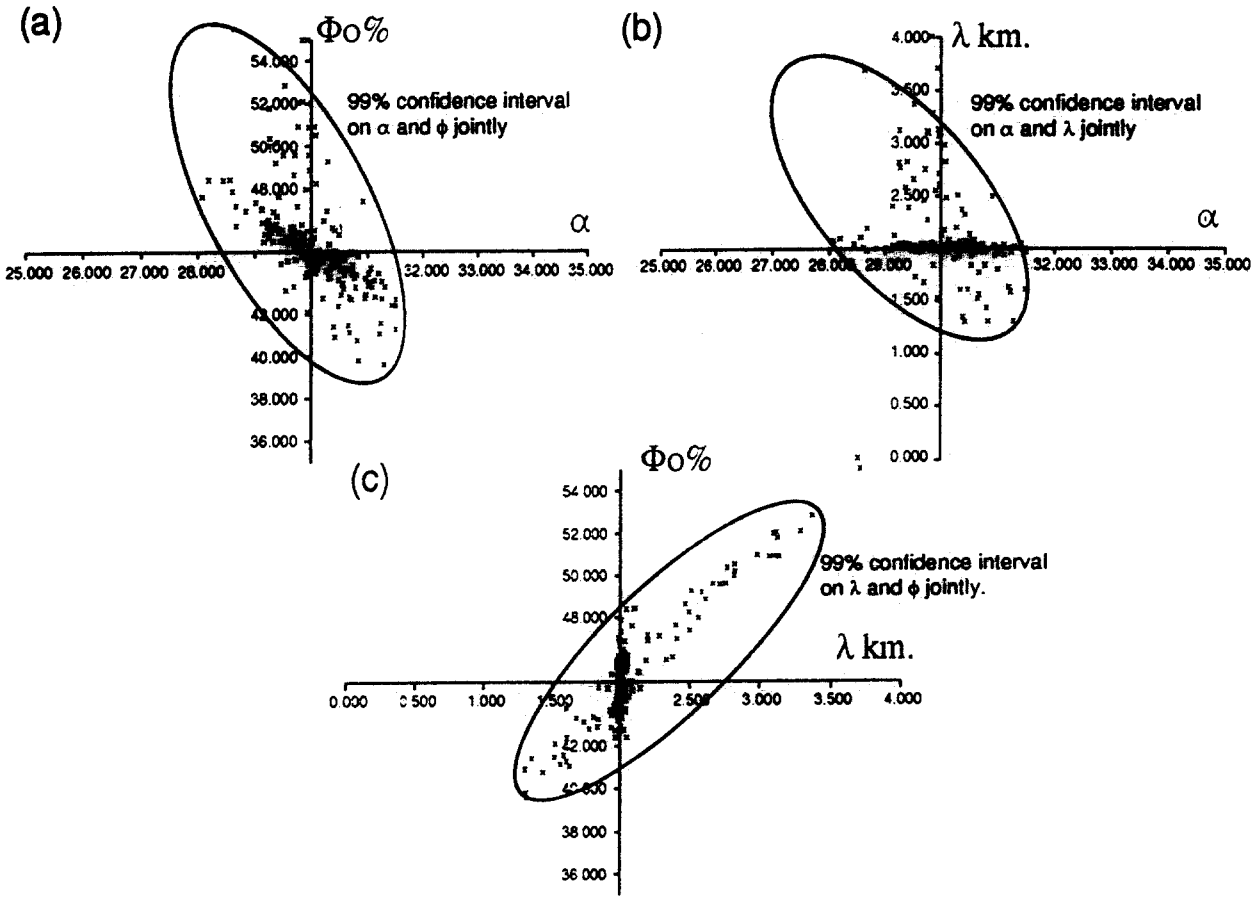

Fig. 8. Three orthogonal sections of solution space which mutually intersect at location of values used in forward model (Fig. 7). Crosses indicate location of solutions found for 200 runs each with different random noise. Circumscribed ellipses delimit 99% confidence regions for each pair of parameters.

argue that the rotational model applies even in the case of a basin-margin fault as long as the footwall deforms internally so as to permit rigid-body rotation of the fault. In other words, the basin margin to a set of dominoes can itself be regarded as a 'soft' domino across which tilting gradually decreases over some distance appropriate to the thickness of the brittle upper crust.

Figure 10 shows how a flexural-cantilever model can be used to predict the observed shapes of tilted blocks in an extensional sedimentary basin. Kusznir *et al.* (1991) argue that this elastic model is an advance on the simple kinematic domino model principally because it avoids space problems at the basin margins. Note, however, that an elastic model still predicts the rotation of normal faults, including the basin-bounding fault. In other words, the relationship between ω, the rotation of each fault and ε, the total extension, is almost identical to the relationship between ω and ε in the simpler domino scheme (Westaway & Kusznir 1993). Thus it is valid to treat all faults as having rotated by the same amount and

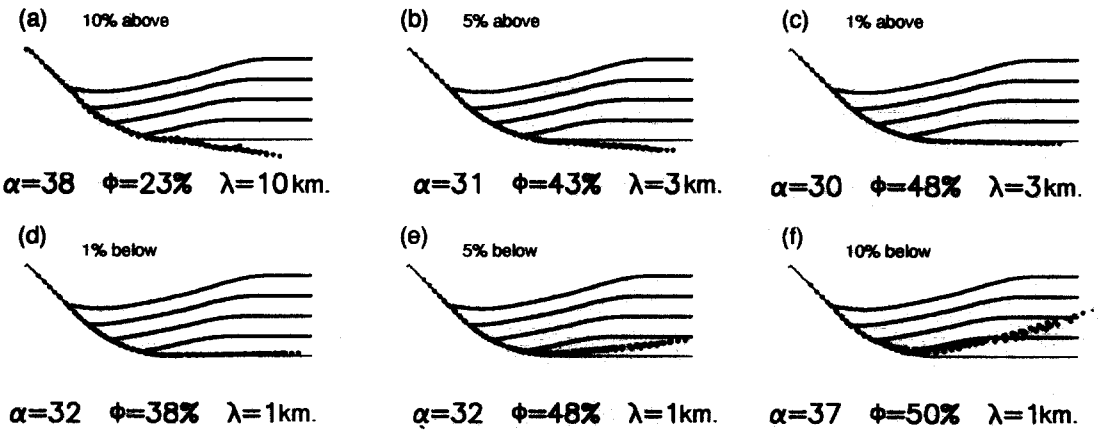

Fig. 9. Investigation of effects of systematic noise by varying the regional levels of each horizon as a percentage of the vertical distance between the top and bottom of the fault. Amount of shift indicated above each figure. Solutions and predicted fault surfaces shown as before (Fig. 1).

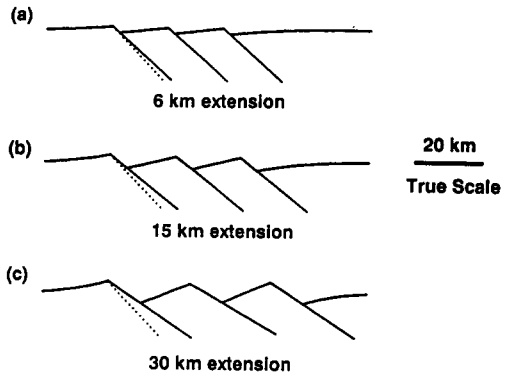

Fig. 10. Flexural cantilever models which illustrate the development of a series of tilted fault-bounded blocks (i.e. dominoes). τ_e = 5 km and dotted line indicates initial geometry of basin-bounding fault on left-hand side. Faults have an initial dip of 45° and are spaced at 15 km intervals. Note increasing block tilt and decreasing dip as extension increases, even for basin-bounding fault.

so fault geometry can be calculated using pre-rift horizons by first unrotating the fault block to its pre-rift orientation. For planar faults, this model is exactly the same as the rigid-domino model but for non-planar faults the hanging wall must still deform internally and some other means must be used to predict this non-planar geometry. The flexural-cantilever model itself cannot be used to determine fault shape since one must assume, *a priori*, that faults have a given shape (planar, listric, etc.).

The most serious difficulty with the flexural-cantilever model is that the shapes of tilted fault blocks within a basin can be fitted using markedly different rheological models, all of which satisfy equations which are biharmonic in form (i.e. can be expressed as $\nabla^4\psi = 0$ where ψ is a potential function; Malvern 1969). Thus syn-rift topography alone cannot be used to discriminate between say, an elastic model and a viscous model. This fundamental drawback is analogous to that encountered when trying to determine the rheological properties of a subducting slab of oceanic lithosphere from bathymetric profiles of the trench and outer rise (e.g. De Bremaecker 1977, Forsyth 1980). As a result, the elastic thickness, τ_e, determined by applying the flexural-cantilever model has no physical meaning. The value usually ascribed to τ_e is merely chosen to ensure that the blocks look as if they are tilted. Such tilting mimics a rigid body rotation but it is in fact an interference effect which becomes more apparent as τ_e is lowered (Fig. 11). If the elastic thickness is smaller than that value which allows the blocks to rotate rigidly, then the fault-bounded blocks must deform by inhomogeneous vertical shear (Westaway & Kusznir 1993). The apparent rotation of faults and blocks within such a deformation field is achieved by pervasive vertical shear. It is unclear to us how faults can be expected to take up significant displacement whilst simultaneously behaving as deforming passive markers.

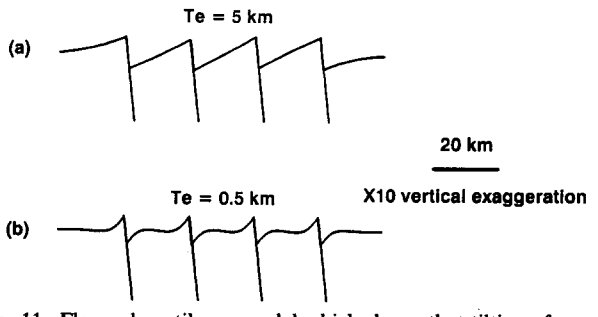

Fig. 11. Flexural cantilever model which shows that tilting of a constant dip results from the interference effect between footwall uplift and hanging wall subsidence. This interference is clearly seen when τ_e is very small (e.g. 0.5 km).

We are wary of using flexural or any other rheological model in this way. Instead, we favour a very simple kinematic scheme based upon the original domino model but modified to allow for internal deformation of each block by shearing and compaction. There are two important reasons for this approach. First, kinematic models based on simple physical principals can be applied without having to make assumptions concerning the rheology of the crust and lithosphere. Secondly, we are interested in tackling the problem of three-dimensional finite deformation in basins and the simple model applied here has proved much easier to generalize for three dimensions (Kerr *et al.* 1993).

APPLICATION TO SEISMIC REFLECTION PROFILES

The examples discussed below were selected because in many cases the fault planes have been imaged at depth. All of them have been modelled by other workers using different models. The range of examples is not intended to be exhaustive but serves to illustrate how the model is applied. In general, we found that the calculated faults agreed with the observed but that the three model parameters, especially the compaction parameters, were often poorly resolved.

Example 1

This first example (Fig. 12), is a growth fault from offshore Louisiana (U.S.A.). Based on seismic character, Xiao & Suppe (1992) were able to correlate eight prominent reflectors across the fault and also interpret the likely location of the main fault surface. The main fault, on the time section, is listric in vertical section and footwall horizons are approximately horizontal. Xiao & Suppe (1992) converted the section to depth and used a rather complicated geometrical construction to forward model deformation by simple shear. They assume that the fault trajectory is known and do not investigate the parameter space.

The inversion algorithm is only applied to depth-converted horizons 5–8 since the upper four have only been displaced by negligible amounts and so do not contribute significantly to the solution. The automatically determined minimum of the misfit function is located at α = 0°, ϕ_o = 0% and λ = 1 km. The significance of ϕ_o = 0% is not that the sediments have zero porosity but means that there are no features in the bed geometry which require differential compaction. Predicted fault surfaces and the fault surface interpreted

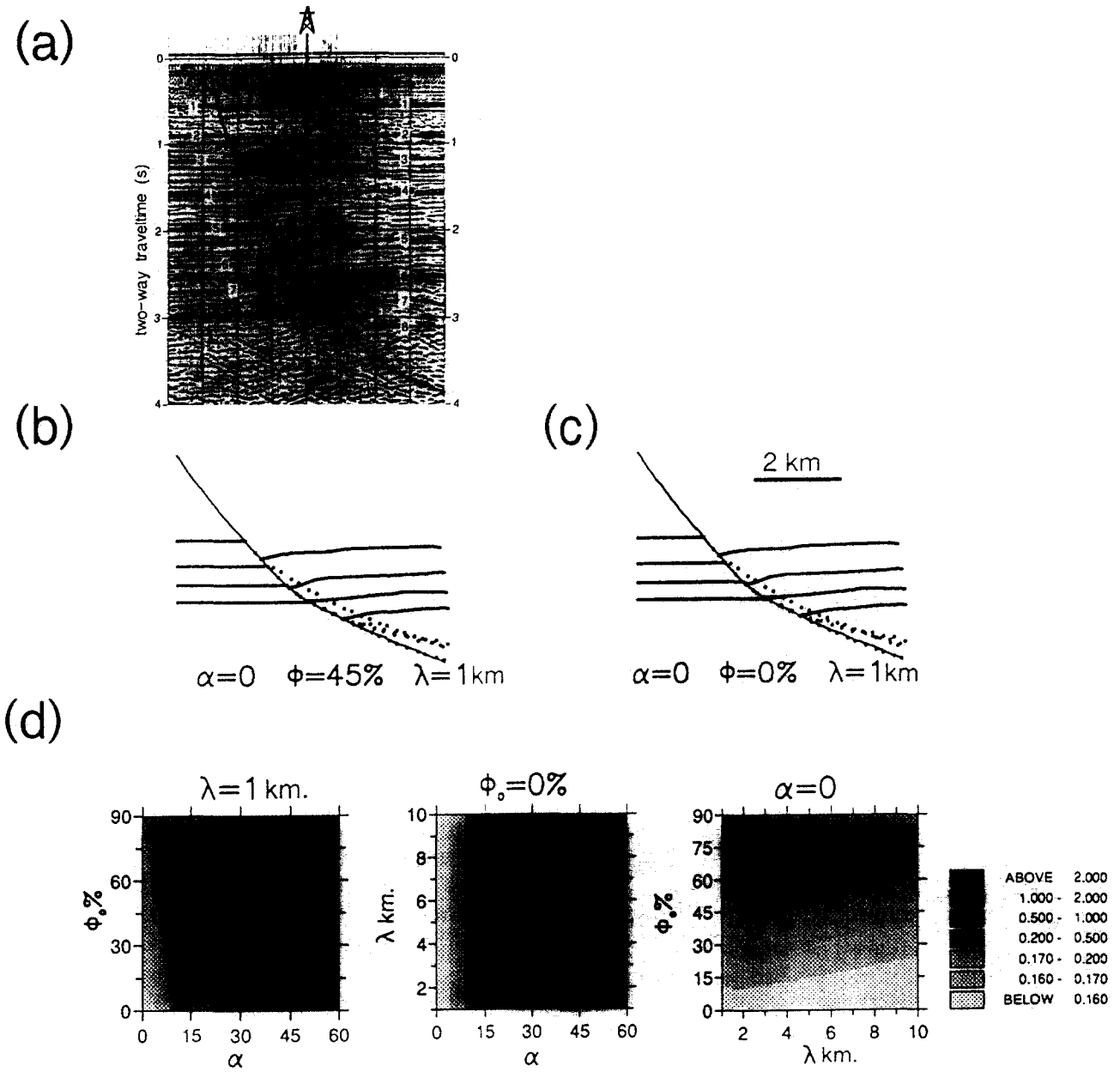

Fig. 12. (a) Interpreted, two-way time, seismic reflection profile (Xiao & Suppe 1992) from offshore Louisiana, U.S.A. (b) & (c) Two inverse models of depth-converted horizons 5–8 in (a). Dotted lines indicate positions of calculated faults at the given parameter values. (d) Three orthogonal plots of misfit function positioned at solution (see text). In each case, the correct solution (i.e. the minimum value of misfit function) lies within lightest shaded area. Contour interval indicated at right-hand side of plots. Next two figures organized in similar fashion.

on the reflection section coincide. The misfit function is plotted on three orthogonal sections (Fig. 12d) located at the values of α, ϕ_0 and λ found by the inversion scheme. These contour plots illustrate the properties of the misfit function around the solution, yielding information about the parameter space which is more important than the actual solution itself. In this case, the minimum is well constrained by α but poorly constrained by ϕ_0 and λ. Figure 12(b) shows that when the value of ϕ_0 is increased in the inverse model to 45% the predicted fault surfaces have a very similar geometry to that they had when $\phi_0 = 0\%$. Hence, as indicated on the contour plots, the inversion scheme is unable to tightly constrain the values of ϕ_0 and λ mainly because the throw of each horizon is small and very little differential compaction has thus occurred.

Example 2

Figure 13(a) shows a listric growth fault from onshore southern Louisiana, U.S.A. (Xiao & Suppe 1992). Only depth-converted horizons 3–6 are used in the inverse algorithm since horizons 1 and 2 have very small displacements. A minimum of the misfit function is located at $\alpha = 0°$, $\phi_0 = 40\%$ and $\lambda = 4$ km. The fault surfaces predicted at these values are similar to the fault surface interpreted on the reflection section (Fig. 13b). Contour plots (Fig. 13c) of the misfit function around the located

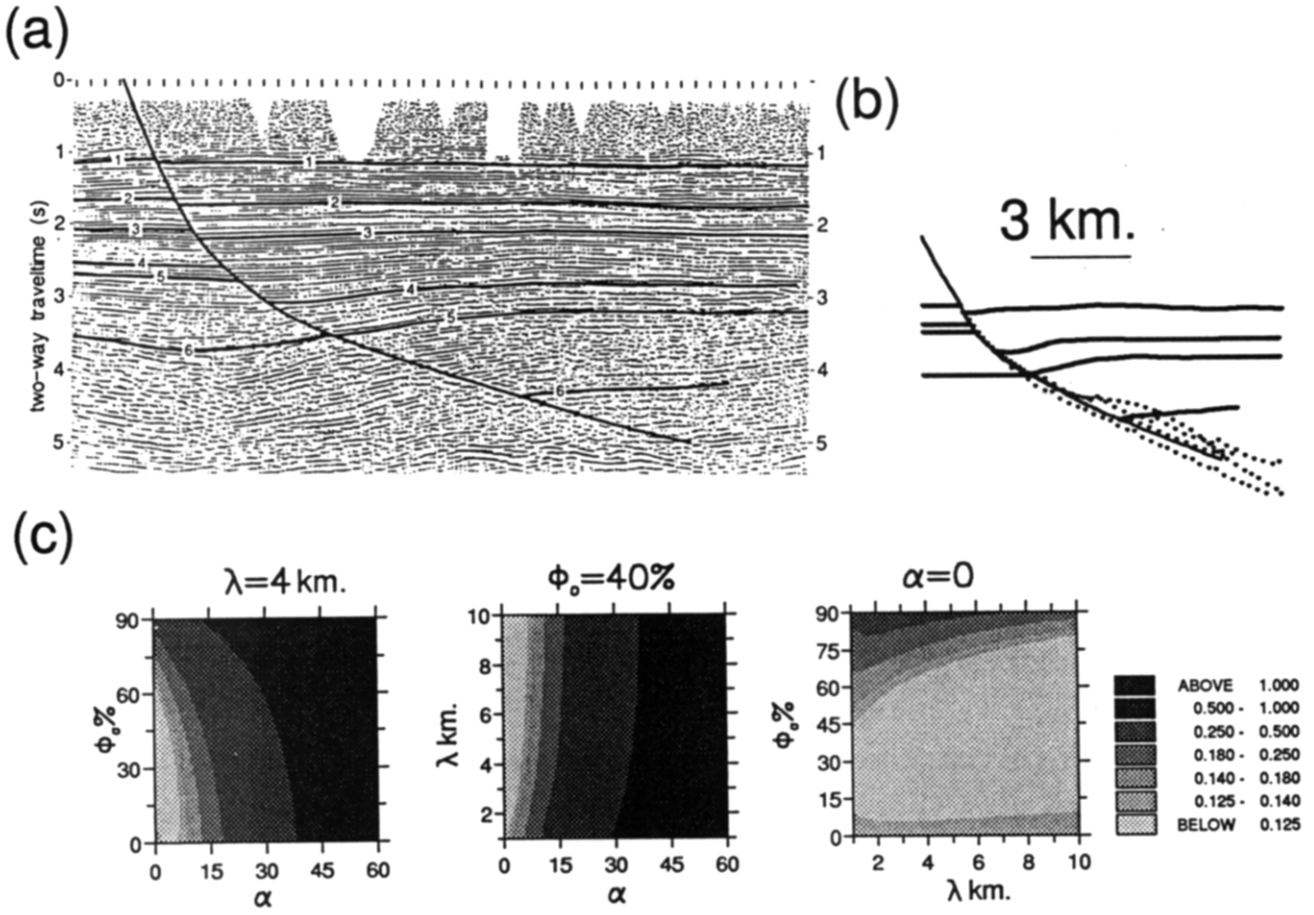

Fig. 13. (a) Interpreted, two-way time, seismic reflection profile (Xiao & Suppe 1992) from onshore southern Louisiana, U.S.A. (b) Inverse model of depth-converted horizons 3–6 in (a). Minimum of misfit function at $\alpha = 0°$, $\phi_o = 40\%$, $\lambda = 4$ km. Calculated fault surface and misfit function (c) shown as before.

solution indicate that the minimum is well constrained by α and badly constrained by the parameters which control compaction ϕ_o and λ.

Example 3

A well defined rollover structure, from the Mississippi Canyon (U.S.A.), is shown on the seismic reflection section in Fig. 14(a) (Xiao & Suppe 1992). Xiao & Suppe (1992) are confident of the correlation of horizons 1–3 from the hanging wall to footwall but were unable to correlate horizons 4–8. Consequently, since levels of horizons within the footwall are used to fix regional levels initially, only horizons 2 and 3 were used to determine fault geometry. Horizon 1 was not included since its displacement is very small, providing little constraint on the fault surface geometry.

Examples 1 and 2 yielded solutions at $\alpha = 0°$ with little or no compaction which is equivalent to applying the 'Chevron construction' (Verrall 1981). This may suggest that allowing the direction of shear to vary between 0° and 60° makes a simple method unnecessarily complicated and it would be sufficient to set α to zero for all applications of the inverse model. Figure 14(b) shows that calculated fault surfaces at $\alpha = 0°$ are not close to the interpreted surface and so blindly setting α to zero provides an unsatisfactory solution.

The inversion scheme, which makes no *a priori* assumptions of the values of α, ϕ_o and λ, automatically located a minimum of the misfit function at $\alpha = 50°$, $\phi_o = 0\%$ and $\lambda = 1$ km. Contour plots of the misfit function around the solution (Fig. 14c) indicate that all three parameters are poorly constrained. It would therefore be appropriate to fix α to any value between 15° and 60°. Predicted fault surfaces, at the solution given by Powell's algorithm ($\alpha = 50°$, $\phi_o = 0\%$ and $\lambda = 1$ km), are not close to the interpreted fault surface and cut the hanging wall stratigraphy (Fig. 14d). However at $\alpha = 25°$, $\phi_o = 0\%$ and $\lambda = 1$ km predicted fault surfaces are close to the actual fault surface (Fig. 14e). Hence deformation can be adequately represented by arbitrarily inclined simple shear ($\alpha = 25°$) but the inversion scheme is unable to automatically identify the most appropriate value of α. Automatic inversion fails in this case because only two closely spaced beds are used and so, irrespective of the deformation parameters, misfit between faults is always small. To obtain a better solution it is advantageous to sample more than two beds over a wider depth range.

If the regional levels of horizons 4–8 are fixed just above the level of the horizons at the right end of the section, all interpreted horizons, excluding horizon 1, can be included in the inversion. Regional levels are fixed at this position in accordance with the gently dipping portion of the main fault at depth (Fig. 14g). A

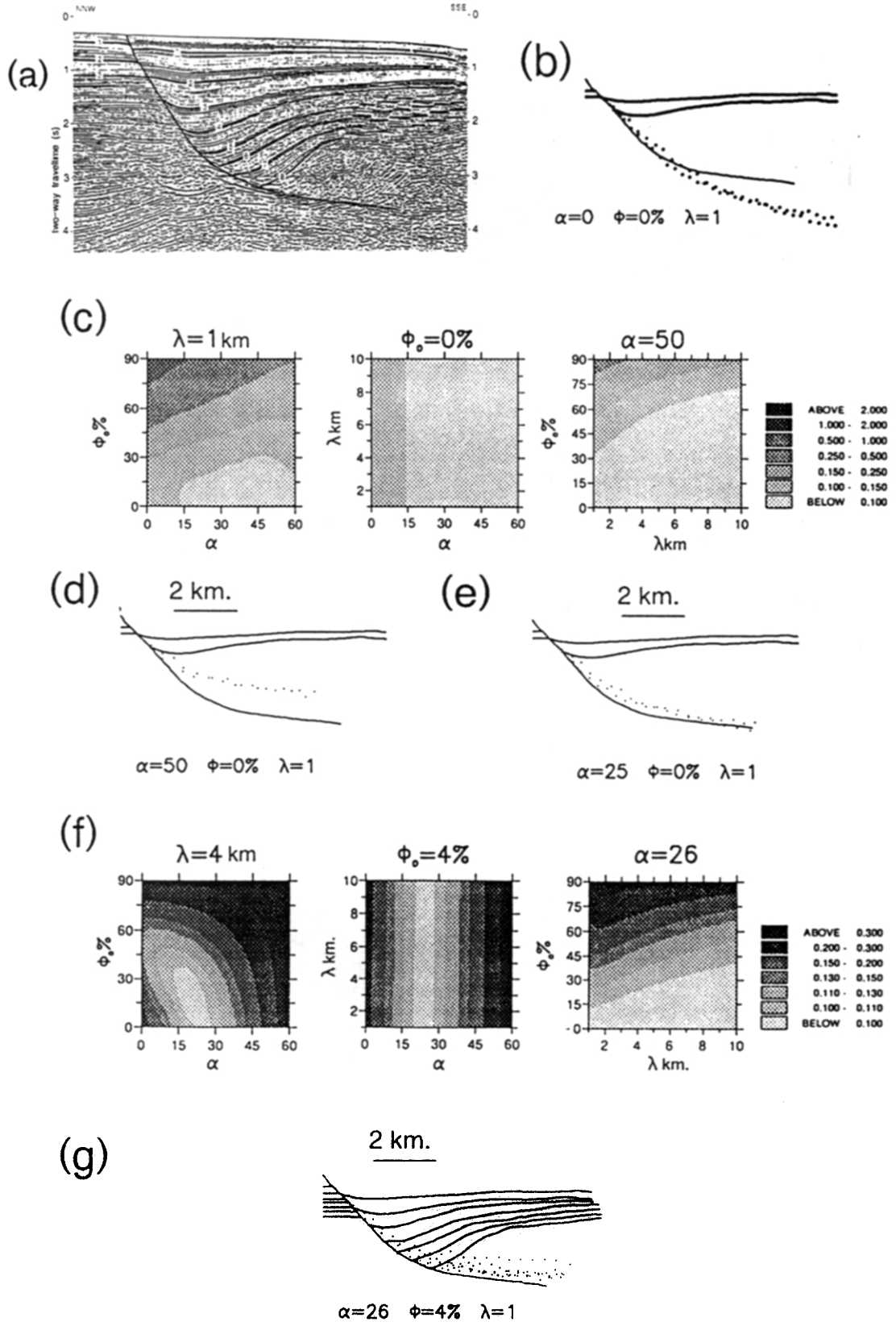

Fig. 14. (a) Interpreted, two-way time, seismic reflection profile (Xiao & Suppe 1992) from Mississippi Canyon (U.S.A.). (c) Misfit function for beds 2 and 3 at retrieved solution. (b), (d) & (e) Inverse models of depth-converted horizons 2 and 3 with parameters set to values given below each plot. (f) Misfit function at solution for beds 2–8. Regional levels indicated in footwall. (g) Inverse model at solution for beds 2–8.

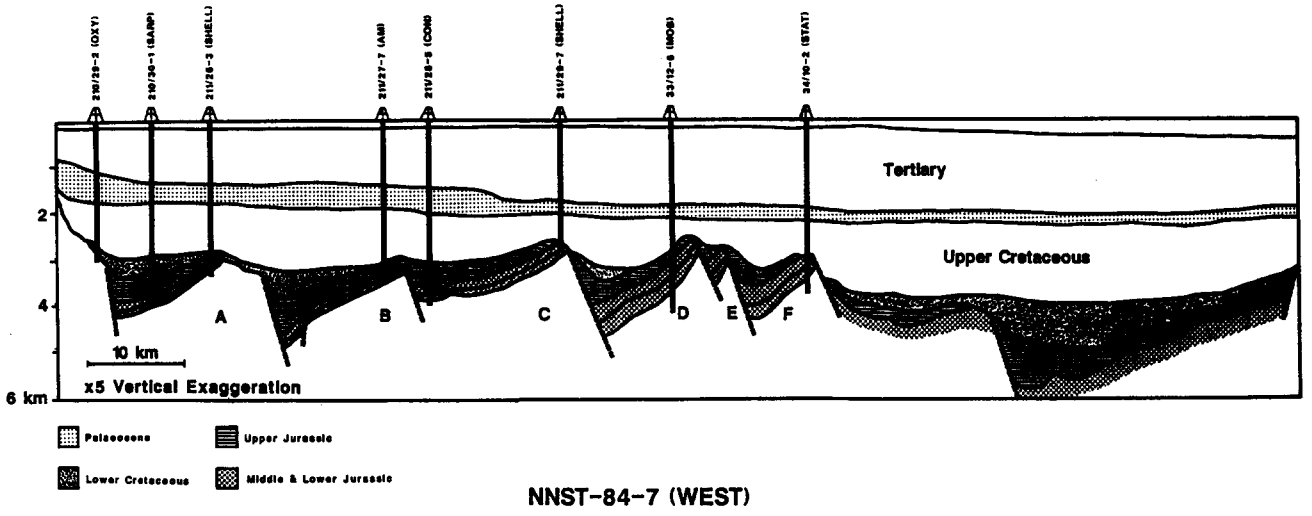

Fig. 15. Depth-converted interpretation of the western portion of NNST-84-7, located at 61°N in North Sea, illustrating structure of East Shetland basin. Original seismic reflection data was generously provided by NOPEC and GECO. See White (1990) for further details.

solution is located automatically at $\alpha = 26°$, $\phi_0 = 4\%$ and $\lambda = 4$ km. Contour plots of the misfit function indicate that the solution is now well constrained by both α and ϕ_0 and poorly constrained by λ (Fig. 14f). All fault surfaces calculated at the solution (Fig. 14g) are slightly shallower than the fault surface interpreted on the reflection section. It is possible that this discrepancy is due to errors in setting regional levels. However, in order to be confident of a solution, the three-dimensional method described by Kerr *et al.* (1993) should be applied to two-dimensional grids of seismic reflection data.

Example 4

All of the examples presented so far are of faults whose dips change considerably with depth. In this section, we show that the inversion model can also be applied to basement-extending normal faults which frequently involve rigid-body rotations about horizontal axes. The four examples shown here are from NNST-84-7, a seismic reflection profile which crosses the East Shetland basin of the northern North Sea from west to east at 61°N. This line is part of a survey shot by the Geophysical Company of Norway (GECO a.s) and Norwegian Petroleum Exploration Consultants (NOPEC a.s) in May 1984. It was interpreted and depth-converted by White (1990; refer to Fig. 15).

Four tilted fault-bounded blocks from this line are modelled (Fig. 16). Middle and lower Jurassic horizons, whose regional levels are fixed at the intersection of footwall horizons and the fault surface, are inverted. Fault blocks A and B are not analysed since Jurassic sediments are completely eroded in their footwalls and so regional levels cannot be determined with sufficient accuracy.

Fault geometries are calculated whilst allowing for differing amounts of anti-clockwise rotation. The misfit at the solution is generally smaller when an anti-clockwise rotation of 5–10° is allowed for (Fig. 16). With no rotation, the predicted fault surfaces are listric and intersect hanging wall strata. With 6° anti-clockwise rotation, the value of the misfit is significantly smaller, yielding approximately planar faults. A listric fault geometry is still predicted for fault D as inversion automatically located a minimum $\alpha = 58°$ which is most likely too high. At lower values of α the amount of misfit is almost the same as at $\alpha = 58°$ and the predicted fault surface is approximately planar, With an allowance for a 10° rotation, the dip of the predicted fault surfaces increase. Therefore provided an anti-clockwise rotation of between 5° and 10° about a horizontal axis is allowed for, the inverse model is able to predict fault geometries which are consistent with what is thought to be the actual geometries of these faults (Yielding *et al.* 1991).

We emphasize again that even though Powell's algorithm can yield $\phi_0 = 0\%$, this value does not imply that the sediments have no porosity. It simply means that very little differential compaction has occurred. Poor control on ϕ_0 results from the same reason.

Example 5

The next example is a major normal fault which separates the Trøndelag Platform from the Halten Terrace (mid-Norway rift; Fig. 17). Roberts & Yielding (1991) applied the flexural-cantilever model of Kusznir *et al.* (1991) to the main boundary fault in order to forward model the footwall deformation. They assumed that the fault was planar and that the footwall deformation could be modelled elastically, despite the fact that this region consists of planar strata which have been broken up by numerous small faults rather than having been deformed into an 'exponential' shape. Here we demonstrate that the arbitrarily inclined shear model can be used to determine the geometry of the main fault surface, provided rigid-body rotation about a horizontal axis is allowed for. The observed footwall deformation probably accommodates the required rigid-body rotation of the main fault.

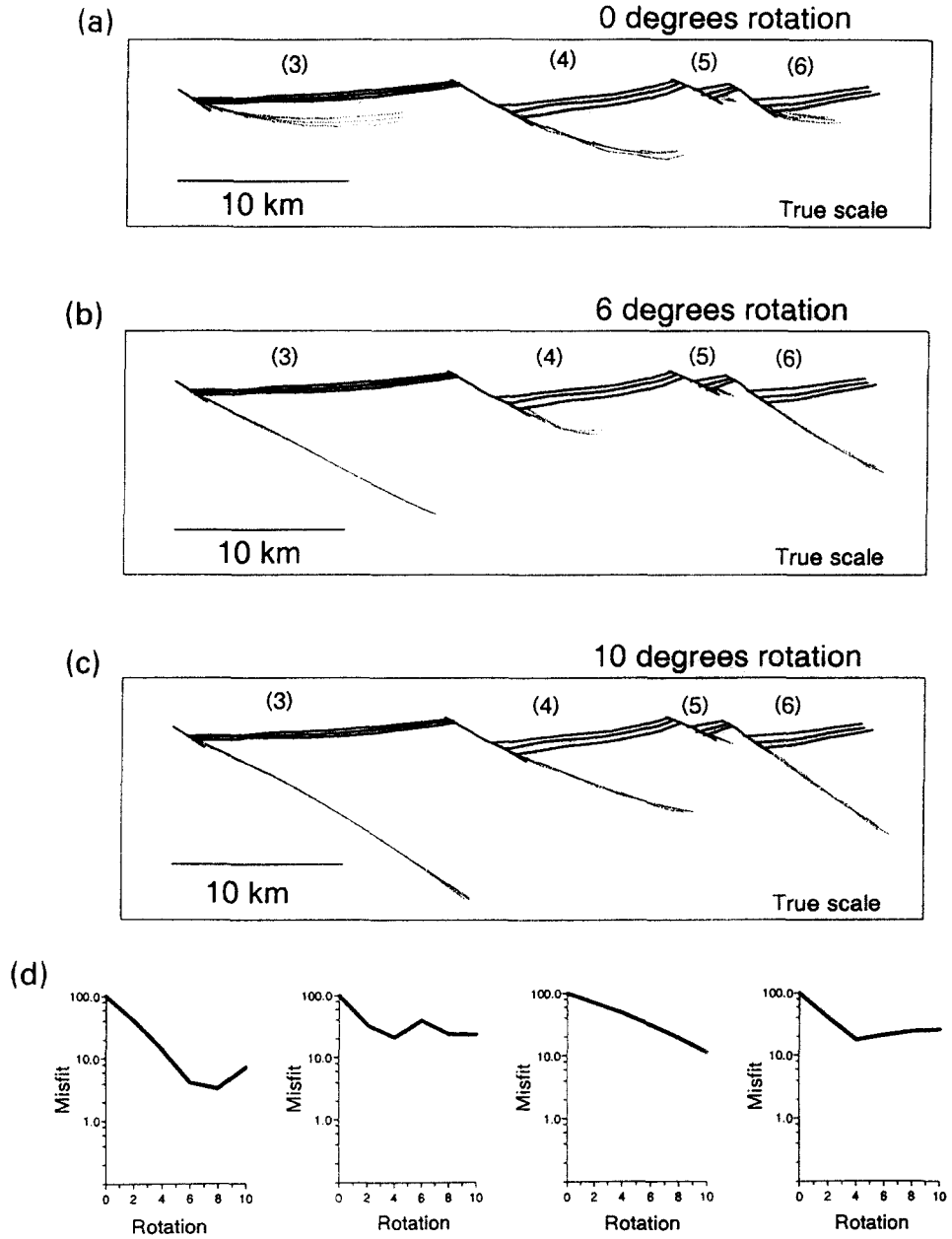

Fig. 16. Results of inverse modelling for four of the normal faults shown in Fig. 15. (a) No allowance for block rotation about horizontal axes. Note large misfit and listric faults which cut deep strata; (b) & (c) allowance made for increasing amounts of block rotation resulting in smaller misfits and approximately planar faults; (d) plots of misfit as a function of rotation for each modelled fault.

Pre-rift Triassic and middle-lower Jurassic marker horizons are used in the inversion. Middle-lower Jurassic sediments are not preserved in the footwall due to erosion following footwall uplift (Roberts & Yielding 1991). We infer the regional level of each bed by projecting the fault surface upwards and placing the thicknesses of Jurassic sediments, observed in the hanging wall, on top of the 'intra' Triassic horizon observed in the footwall. Figure 17(b) shows the misfit, at the solution, plotted against clockwise rotation. The minimum misfit is obtained with a rotation of 10°. The fault surfaces predicted with a rotation of 0°, 5° and 10° are shown, by the dotted lines, in Fig. 17(c). With a rotation of 10° predicted fault surfaces are planar with dips of approximately 45°. This is consistent with the interpretation of Roberts and Yielding (1991). Values of the three model parameters are poorly resolved.

Example 6

Our final example comes from the Horda platform, offshore Norway (Fig. 18a). Geometries of the main fault surface and the horizons were interpreted, migrated and depth-converted by Yielding *et al.* (1991). The three upper Jurassic horizons are used in the inversion scheme. The minimum misfit, at the solution, is obtained with no rotation (Fig. 15b). Figure 15(c) shows predicted fault surfaces, at the solutions, allowing for rotations of 0°, 5° and 10°. With no rotation the predicted fault surfaces are close to the interpretation of Yielding

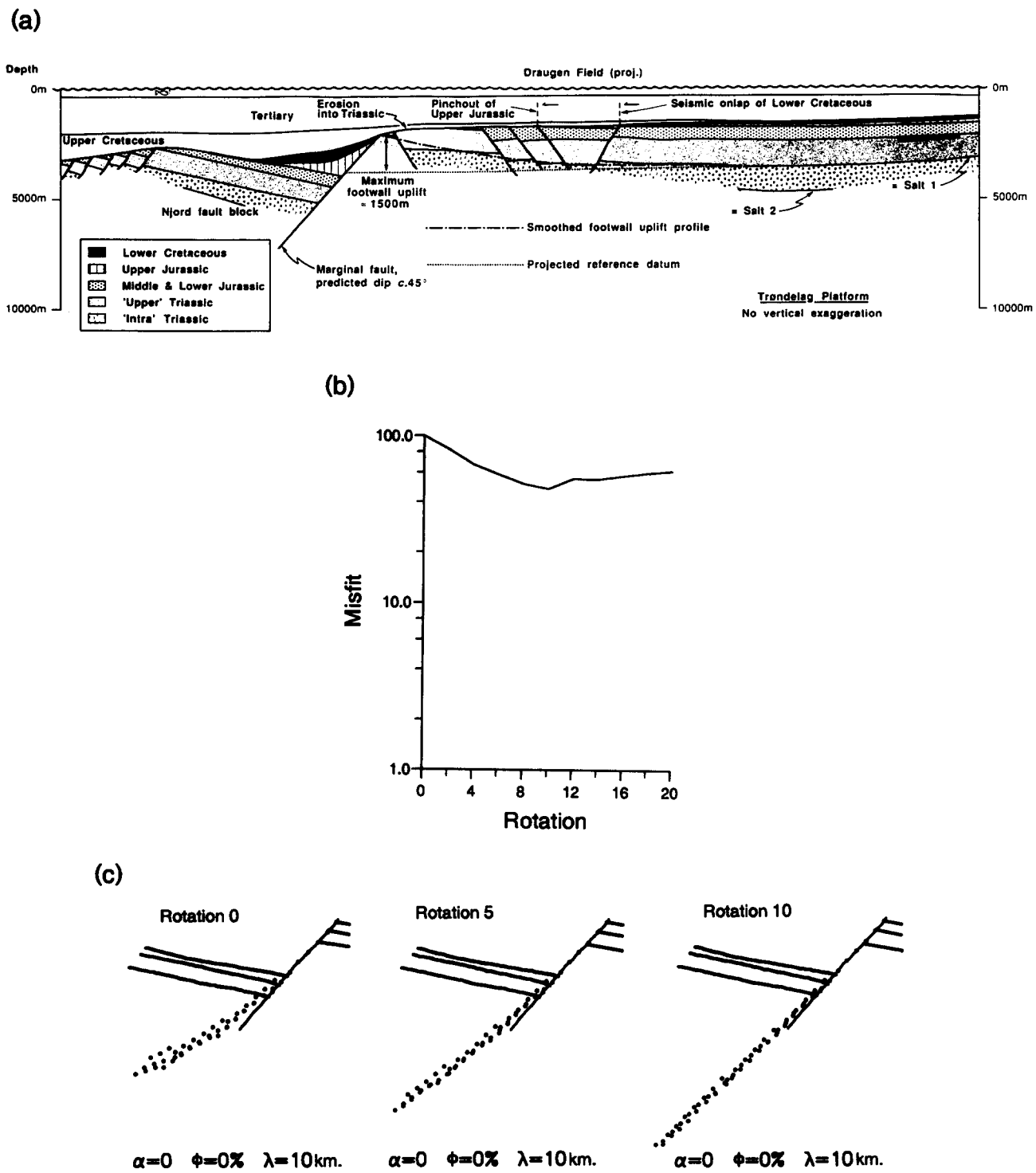

Fig. 17. (a) True scale section across the Trøndelag Platform/Halten Terrace basin margin (Norwegian sector: Roberts & Yielding 1991). Note that smoothed footwall uplift profile cuts across strata which are, in fact, faulted. (b) Plot of misfit vs rotation for main fault in (a); note minimum 10° rotation. (c) Dotted lines are predicted faults at solution indicated by parameter values for different amounts of clockwise rotation. All three parameters are very poorly constrained in this inversion.

et al. (1991). Hence arbitrarily inclined simple shear is representative of hanging wall deformation.

CONCLUSIONS

The most important conclusion is that the arbitrarily inclined shear model is applicable to normal faults of any shape ranging from surficial listric faults to major 'domino' style planar (?) faulting. Where rotations about horizontal axes have occurred and no allowance for such rotations have been made, then listric faults with large misfit values are predicted. Approximately planar faults with dips between 30° and 45° are predicted for domino style faults in the North Sea if the appropriate amount of rotation (5–10°) is used. These results are

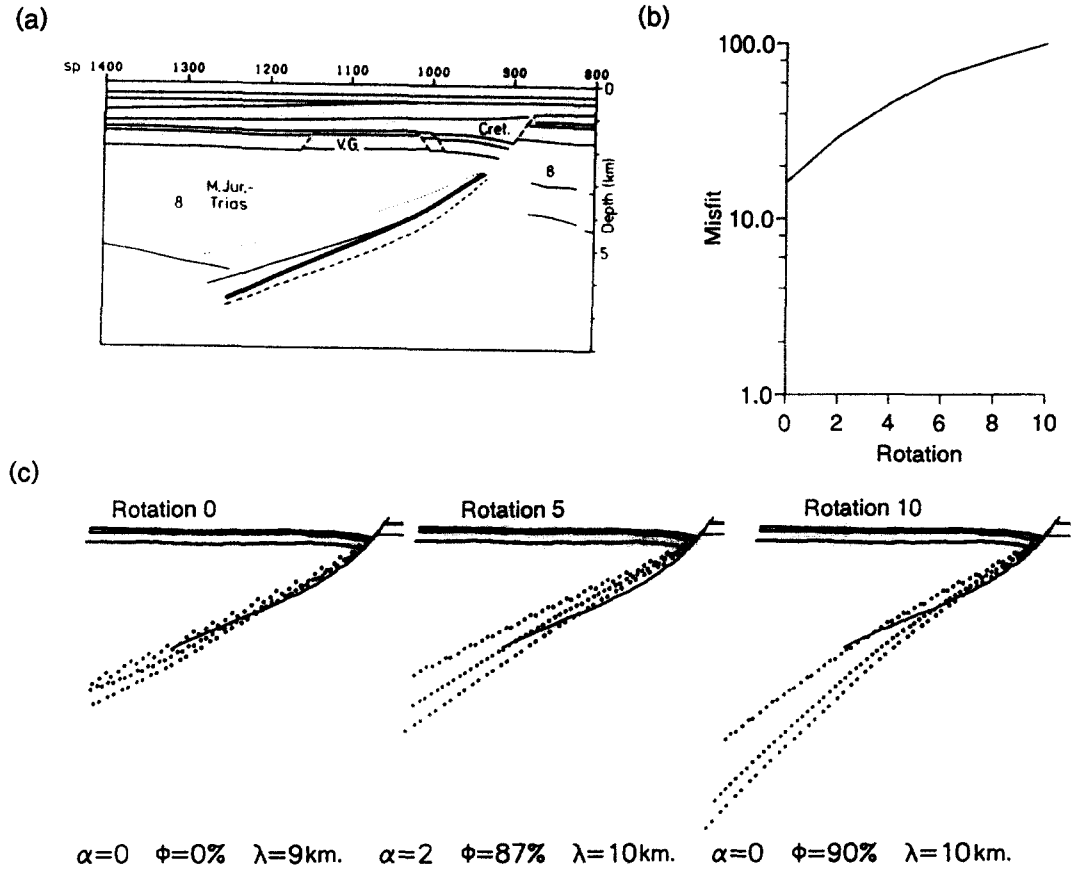

Fig. 18. (a) True-scale section across fault on Horda platform, northern North Sea (Yielding *et al.* 1991). Dotted, dashed and bold lines show migration for fault-plane reflection for different velocity structures (see Yielding *et al. loc. cit.*). (b) Plot of misfit vs rotation for main fault in (a). (c) See Fig. 17 for details.

in accord with seismological studies of large-magnitude earthquakes in regions of active extension (Jackson 1987).

We have also investigated a variety of complications which may arise in applying the model to data in sedimentary basins. First, synthetic flexural modelling demonstrates that if fault surfaces change geometry relative to the hanging wall during deformation, the misfit function has large values and is featureless in the vicinity of the automatically determined solution. Such negative results are very useful since they indicate that one or more of the underlying assumptions is invalid. Secondly, the forward model was adapted to model the axis of shortening for compaction both vertical and parallel to the fault surface. In both cases the inverse model, which by necessity models the axis of shortening parallel to the direction of shear, was still able to adequately represent deformation and predict the correct fault surface. Hence, contrary to the reservations of Waltham (1990), constraining compaction to be parallel to the direction of shear is an acceptable approximation. Thirdly, the effects of post-rift burial have been investigated and are shown to be negligible.

We have also examined the effects of both random and systematic noise and have established empirically that the inversion procedure is well-posed (Parker 1977). However, care is required in defining the regional levels of the deformed hanging wall strata across the fault into the footwall. If regional levels are selected below their actual positions then the predicted faults will intersect the hanging wall strata.

Throughout, we have assumed that the regional dip of all horizons is zero (i.e. the beds are initially horizontal). When the beds have an initial dip the method can be simply adapted (White 1992). Oblique extension may have been significant in some of the example presented here. Consequently, to gain maximum confidence in a solution the three-dimensional method (Kerr *et al.* 1993, in preparation) should be applied. Inverse theory is used to determine both the three-dimensional fault geometry and the direction of extension within the horizontal plane.

Acknowledgements—H.G.K. gratefully acknowledges a Petroleum Science and Technology Institute (P.S.T.I.) studentship and generous provision of computational facilities. R. Ratliff, A. Roberts, J. Wheeler and G. Yielding provided thorough reviews. Petroleum Science and Technology Institute Contribution 011 and Department of Earth Sciences Contribution 3609.

REFERENCES

Bally, A. W. 1983. Seismic expression in structural styles. *Bull. Am. Ass. Petrol. Geol., Stud. Geol. Ser.* **15.**

Birkhoff, G. 1955. *Hydrodynamics*. Dover Publications, New York.

De Bremaecker, J. C. 1977. Is the oceanic lithosphere elastic or viscous? *J. Geophys. Res.* **82,** 2001–2004.

Forsyth, D. W. 1980. Comparison of mechanical models of the oceanic lithosphere. *J. geophys. Res.* **85,** 6364–6368.

Gibson, J. R., Walsh, J. J. & Waterson, J. 1989. Modelling of bed

contours and cross-sections adjacent to planar normal faults. *J. Struct. Geol.* **11**, 317–328.

Jackson, J. A. 1987. Active normal faulting and crustal extension. *Geol. Soc. Spec. Publ. Lond.* **28**, 3–17.

Jankhoff, K. 1945. Changes in ground level produced by the earthquakes of April 14–18, 1928 in southern Bulgaria. In: *Tremblements de terre en Bulgarie*, Nos 29–31. *Institut meteorologique central de Bulgarie, Sofia*, 131–136.

Kerr, H. G. & White, N. 1992. Laboratory testing of an automatic method for determining normal fault geometry at depth. *J. Struct. Geol.* **14/7**, 873–885.

Kerr, H. G., White, N. & Brun J. P. 1993. An automatic method for determining 3-D normal fault geometries. *J.Geophys. Res.* **98**, 17837–17857.

King, G. C. P., Ouyang, Z. X., Papadimitriou, P., Deschamps, A., Gagnepain, J., Houseman, G., Jackson, J. A., Soufleris, C. & Virieux, J. 1985. The evolution of the Gulf of Corinth (Greece): an aftershock study of the 1981 earthquakes. *Geophys. J. R. astr. Soc.* **80**, 677–693.

Kusznir, N. J., Marsden, G. & Egan, S.S. 1991. A flexural cantilever simple-shear/pure-shear model for continental lithosphere extension: applications to the Jeanne d'Arc Basin, Grand Banks and Viking Graben, North Sea. *Geol. Soc. Spec. Publ. London.* **56**, 41–60.

Le Pichon, X. & Sibuet, J. C. 1981. Passive margins: a model of formation. *J. geophys. Res.* **86**, 3708–3720.

Lyon-Caen, H. & Molnar, P. 1986. Constraints on the structure of the Himalaya from an analysis of gravity anomalies and a flexural model of the lithosphere. *J. geophys. Res.* **88**, 8171–8191.

Malvern, L. E. 1969. *Introduction to the Mechanics of a Continuous Medium*. Prentice-Hall, New Jersey.

McKenzie. D. P. & Jackson, J. A. 1983. The relationship between strain rates, crustal thinning, paleomagnetism, finite strain and fault movement within a deforming zone. *Earth Planet Sci. Lett.* **65**, 182–202.

Myers, W. B. & Hamilton, W. 1964. Deformation accompanying the Hagben Lake earthquake of 17 August 1959. *Geol. Surv. Prof. Pap. U.S.* **435**, 55–98.

Parker, R. L. 1977. Understanding inverse theory. *Earth Planet Sci. Lett.* **5**, 35–64.

Press, W. H., Flannery, B. P., Teukolsky, S. A. & Vetterling, W. T. 1986. *Numerical Recipes: The Art of Scientific Computing*. Cambridge University Press, New York, 294–301.

Proffett, J. M. Jr. 1977. Cenozoic geology of the Yerington district, Nevada, and implications for the nature and origins of the Basin and Range faulting. *Bull. Geol. Soc. Am.* **88**, 247–266.

Ramsay, J. G. 1967. *Folding and Fracturing of Rocks*. McGraw-Hill, San Francisco.

Ransome, P. F., Emmons, W. H. & Garrey, G. H. 1910. Geology and ore deposits of the Bullfrog District, Nevada. *Bull U.S. Geol. Surv.* **407.**

Richins, W. D., Pechman, J. C., Smith, R. B., Langer, C. J., Goter, S. K., Zollweg, J. E. & King, J. J. 1987. The 1983 Borah Peak, Idaho, earthquake and its aftershocks. *Bull. seism. Soc. Am.* **77/3** 694–723.

Richter, C. F. 1958. *Elementary Seismology*. W. H. Freeman, San Francisco.

Roberts, A. G., Yielding, G. & Freeman, B. 1990. The geometry of normal faults. *J. geol. Soc. Lond.* **147**, 185–187.

Roberts, A. G. & Yielding, G. 1991. Deformation around basin-margin faults in the North Sea/mid-Norway rift. *Geol. Soc. Spec. Publ. Lond.* **56**, 61–78.

Sclater, J. G. & Christie, P. A. F. 1980. Continental stretching; an explanation of the post-mid Cretaceous subsidence of the Central North Sea Basin. *J. geophys. Res.* **85**, 3711–3739.

Soufleris, C., Jackson, J. A., King, G. C. P., Spencer, C. & Scholz, C. H. 1982. The 1978 earthquake sequence near Thessaloniki (northern Greece). *Geophys. J. R. astr. Soc.* **68**, 429–458.

Stein, R. S. & Barrientos, S. E. 1985. Planar high angle faulting in the Basin and Range: geodetic analysis of the 1980 Borah Peak, Idaho, earthquake. *J. geophys. Res.* **90**, 11355–11366.

Verrall, P. 1981. Structural interpretation with applications to North Sea problems. *Joint Assoc. Petrol. Explor. Courses* **3**, 1–156.

Waltham, D. 1990. Finite difference modelling of sand-box analogues, compaction and detachment-free deformation. *J. Struct. Geol.* **12**, 375–381.

Wernicke, B. & Burchfiel, B. C. 1982. Modes of extensional tectonics. *J. Struct. Geol.* **4/2**, 105–115.

Westaway, R. & Kusznir, N. 1993. Fault and bed 'rotation' during continental extension: block rotation or vertical shear? *J. Struct. Geol.* **15**, 753–770.

White, N. 1990. Does the uniform stretching model work in the North Sea? In: *Tectonic evolution of the North Sea Rifts* (edited by Blundell, D. J. & Gibbs, A. D.). Oxford Science Publications, Oxford.

White, N. 1992. Determining normal fault geometry. *J. geophys. Res.* **97**, 1715–1733.

White, N., Jackson, J. A. & McKenzie, D. P. 1986. The relationship between the geometry of normal faults and that of the sedimentary layers in their hanging walls. *J. Struct. Geol.* **8**, 879–909.

Whitten, C. A. 1957. Geodetic measurements in the Dixie Valley area. *Bull. seism. Soc. Am.* **47**, 321–325.

Wood, R. J. 1981. The subsidence history of CONOCO well 15/30-1, central, North Sea. *Earth Planet Sci. Lett* **54**, 306–312.

Xiao, H. & Suppe, J. 1992. The origin of rollover. *Bull. Am. Ass. Petrol. Geol.* **76/4**, 509–529.

Yielding, G., Badley, M. E. & Freeman, B. 1991. Seismic reflections from normal faults in the northern North Sea. *Geol. Soc. Spec. Publ. Lond.* **56**, 79–89.